ENERGY SOURCES, PART B: ECONOMICS, PLANNING, AND POLICY

Uncertainty Quantification for the Planning of Offshore Wind Farms Using Monte Carlo and Sparse Grid

Pascal Richter[a*], Jannick Wolters[a] and Martin Frank[a]

[a]Karlsruhe Institute of Technology (KIT), Steinbuch Centre for Computing, Karlsruhe, Germany

ARTICLE HISTORY

Compiled August 29, 2020

WORD COUNT

7853 words

ABSTRACT

The power produced by an offshore wind farm is subject to uncertainties such as volatile wind, turbine performance wear, and availability losses. Knowledge about the stochastic distribution of the power production is crucial for the planning stage of wind farms as well as later for their performance improvement. It is equally important to understand how uncertainties propagate through the models and ultimately how sensitive the predicted energy production is with respect to these uncertainties.

Due to the multitude of uncertainties, a complete analysis requires high dimensional numerical integration techniques to determine these sensitivities. Such an analysis has not been done in the literature for the entire set of uncertainties. In this work, for the first time, a thorough analysis of all uncertainties is provided, modeled by years of collected data of existing wind farms. To highlight differences in wind park layouts, the analysis is performed on the three wind farms *Horns Rev 1*, *DanTysk* and *Sandbank*. Starting from a set of nine uncertain parameters, the sensitivity analysis reveals four important candidates, allowing the other parameters to be neglected in future measurement data acquisitions and sensitivity analysis processes. Furthermore, several Uncertainty Quantification techniques are compared

∗ Corresponding author
Email address: pascal.richter@kit.edu (P. Richter)

to provide recommendations for future projects.

KEYWORDS

Offshore wind farm; Uncertainty Quantification; Quasi-Monte Carlo; Stochastic Collocation; Sensitivity Analysis

1. Introduction

The computation of the annual energy production in offshore wind farms depends on a large set of parameters. Most of these parameters have a high level of uncertainty due to the impossibility of performing ideal measurements on volatile wind, the occurrence of material fatigue which influences the performance wear, and other uncertainties such as availability losses. In order to make reasonable predictions for the wind farm energy production, it has to be determined how this value can vary in relation to changes in the uncertainty parameters.

Few publications have considered uncertainties in parameters for wind farm simulations. Lackner and Elkinton (2007) listed a set of wind farm parameters which have an influence on the uncertainty of predicting the energy production. Murcia, Réthoré, Hansen, Natarajan, and Sørensen (2015) analyzed the influence of measurement uncertainties in some of these parameters in order to check for modeling errors. Foti, Yang, and Sotiropoulos (2017) on the other hand focused on two different uncertainties and directly analyzed their influence on the total power production. Rinker (2016) investigated the sensitivity of a single turbine for four parameters which are inflicted with uncertainties. Ashuri, Zhang, Qian, and Rotea (2016) investigated the levelized cost of electricity of a single turbine while considering up to four uncertain parameters. Padrón, Stanley, Thomas, Alonso, and Ning (2016) used polynomial chaos to compute the stochastic effect of wind direction and wind speed on the annual energy production in wind farms.

The novelty of this paper lies in the simultaneous sensitivity analysis for a large set of uncertainties which is based on real world data for multiple offshore wind farms. Having an insight into the strength of these parameter sensitivities could greatly improve the planning stage of future wind parks as e.g. on-site measurements could be focused on the most sensitive parameters. We develop a stochastic model to investigate the impact of nine uncertain input parameters. Several different numerical integration techniques are investigated, which are used for the propagation of the uncertainty parameters through the model. A sensitivity analysis is performed with the most suitable mathematical method to determine the most influential uncertainties on different cost function. We use extensive data to model uncertainties sourced from business operations, in a case study featuring different wind farm layouts.

The outline of this paper is structured as follows: Section 2 describes the deterministic model which we use in order to compute the annual energy production. This involves sub-models for the wake computation, the power generation, and costs. In Section 3 the whole model is extended by introducing randomness into the input parameters to get a stochastic model. Section 4 introduces the Uncertainty Quantification methods starting with the classical Monte Carlo method, followed by its derivations such as the quasi-Monte Carlo and finally the Stochastic Collocation method. The performance of each method will be discussed. Subsequently one of these methods will be recommended based on the presented stochastic model. The stochastic model and the Uncertainty Quantification methods from these two sections are then used in Section 5 where the parameter sensitivities w.r.t. different cost functions is investigated. All results will afterwards be summarized in Section 7.

2. Deterministic Model for the Annual Energy Production in Wind Farms

The annual energy production (AEP) in wind farms is computed by three sub-models which describe the wind, wake, and power generation in a wind farm. The temporal integration of gross produced power is computed by considering the measurements of wind speed and wind direction within one year. For each wind direction and each wind speed, the power produced by the wind farm needs to be computed where the integral over all directions yields the produced energy. This value is then used in a cost model to describe economic quantities, as shown in Figure 1. In the following all sub-models are described.

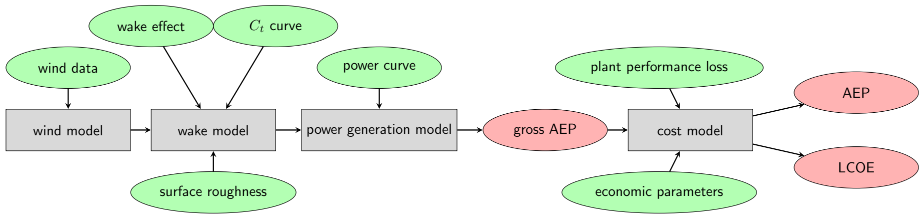

Figure 1.: Structure of the offshore wind farm model. Input parameters are highlighted in green. These parameters are also later used for the uncertainty quantification. Possible outputs of the wind farm model (highlighted in red) are the annual energy production (AEP) and the levelized cost of electricity (LCOE).

2.1. *Wind Model*

Starting from the raw energy source, wind is quantified by thousands of measurements of wind direction and wind speed. Figure 2 shows a clustered wind direction distribution over a time period of eight years. The distribution is divided into several sectors, standing for the cardinal points and representing the probability of the wind direction by the size of each sector. Furthermore, for each wind direction sector, the distribution of wind speed is considered independently.

The classical approach is to model the raw measurement data by a Weibull distribution which is fitted to the data using a maximum likelihood estimation, see Carrillo, Cidrás, Díaz-Dorado, and Obando-Montaño (2014),

$$\mathcal{W}(u;\lambda,k) = \left(\frac{k}{\lambda}\right) \cdot \left(\frac{u}{\lambda}\right)^{k-1} \cdot \exp\left(-\left(u\cdot\lambda\right)^{k}\right), \qquad (1)$$

where $\lambda > 0$ is the scale parameter and $k > 0$ is the shape parameter of the Weibull distribution, as plotted in Figure 3.

In the following sections we will refer to the overall model as deterministic, which means that the input parameters are not subject to any kind of uncertainty.

For the simulation of a wind farm we need to consider each wind direction sector and a certain number of wind speeds. It is clear, that the model becomes more precise by increasing the number of wind sectors N_{dir} and wind speeds N_{speed}.

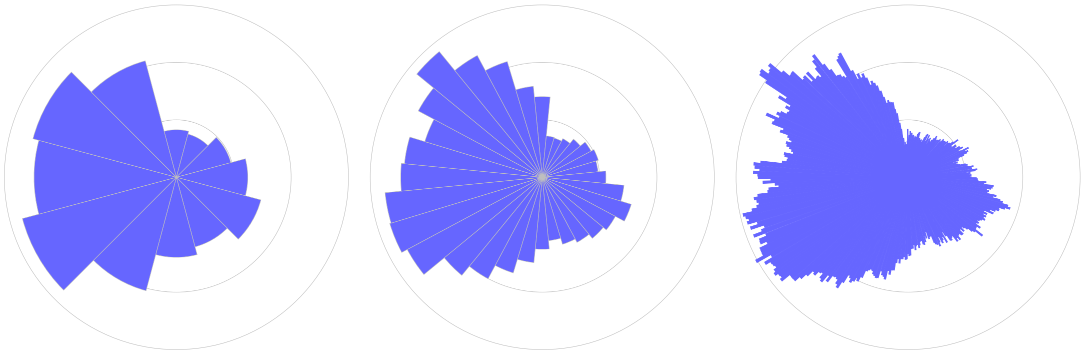

(a) 12 sectors (b) 32 sectors (c) 360 sectors

Figure 2.: Wind direction measurements at the FINO3 research platform in the North Sea, about 80 km away from the German island Sylt. The measurements at a 100 m height taken over eight years from January 2010 to December 2017 are clustered into N_{dir}=12, 32, and 360 direction sectors.

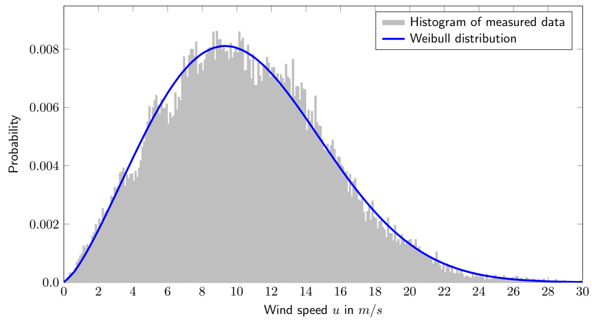

Figure 3.: Wind speed measurements at the FINO3 research platform at a height of 100 m for the eight years from January 2010 to December 2017 for the western wind direction sector (255° to 285°). The data is fitted by a Weibull distribution using the maximum likelihood estimation.

2.2. *Wake Model*

In an offshore wind farm, several wind turbines are arranged in a predefined region. The wind passing the turbine blades generates a wake behind each wind turbine, which is responsible for wind speed reductions for subsequent wind turbines. The task of a wake model is to compute this impeded velocity field behind each wind turbine.

In literature, one can find many different models which describe the wake effect. The first notable wake model was developed by N. O. Jensen (1983) and Katic, Højstrup, and Jensen (1986), which is called *PARK model*. Further developments are the *Eddy-Viscosity wake model* by Ainslie (1988) and some extensions by Lange, Waldl, Guerrero, Heinemann, and Barthelmie (2003); Larsen et al. (2007), the *Deep-array wake model* by Brower and Robinson (2012), a *linearized Reynolds-averaged*

Navier–Stokes model by Ott (2009), and *Large Eddy Simulations* by Stovall, Pawlas, and Moriarty (2010).

In this paper we focus on the *PARK model*, which is mainly used in commercial software tools, because the velocity deficit calculated by the model has a top-hat shape which allows for a simple and efficient computation. This efficiency is also needed in the context of this paper as the high dimensional integration, required to obtain the statistical quantities of interest, requires lots of evaluations of the model and therefore is not feasible with full CFD Navier-Stokes simulations. Furthermore, investigations by Barthelmie et al. (2006) show that the computations are quite accurate compared to other more detailed models, such as the k-ε turbulence model which is based on a parabolized Navier–Stokes model by Schepers (2003). It is well known that PARK overestimates wake losses and is not considering deep array effects of wind farms, see Gaumond et al. (2014); Pillai, Chick, and Laleu (2014). Therefore we consider an additional loss term ℓ_{wake} in the model.

The velocity deficit inside the wake only changes in down stream direction. The wake radius in the PARK model grows with a constant factor $k := 0.5/\ln(z/z_0)$, which depends on the hub height z of the turbine and the surface roughness z_0. The wake diameter $D_w(x)$ grows linearly by $2k$, as illustrated in Figure 4. For an inflow velocity u_0, the wake velocity $u_w(x)$ at any point inside the wake of a turbine with rotor diameter D is given by

$$u_w(x) = (\ell_{\text{wind}} \cdot u_0) - \frac{1 - \sqrt{1 - C_t(\ell_{\text{wind}} \cdot u_0)}}{\left(1 + \frac{2x}{D} \cdot \frac{1}{2\ln(z/z_0)}\right)^2} \cdot \ell_{\text{wake}} \cdot (\ell_{\text{wind}} \cdot u_0), \tag{2}$$

where the last fraction describes the velocity deficit. The velocity dependent thrust coefficient of the turbine $C_t(u_0)$ is a characteristic property of the turbine type and thus needs to be provided by the manufacturer of the wind turbine (Figure 5). The loss parameter ℓ_{wake} is used to consider wake effect losses due to internal turbine arrays, external turbines, and future developments in the vicinity of the wind farm. Furthermore, we consider wind speed losses ℓ_{wind} due to turbulence, off-yaw axis winds, inclined flow, and high shear wind flow. Loss parameters are mainly based on experience and thus are used to make the developed model more realistic, by closing the gap between turbine power curve test conditions and actual conditions at the site.

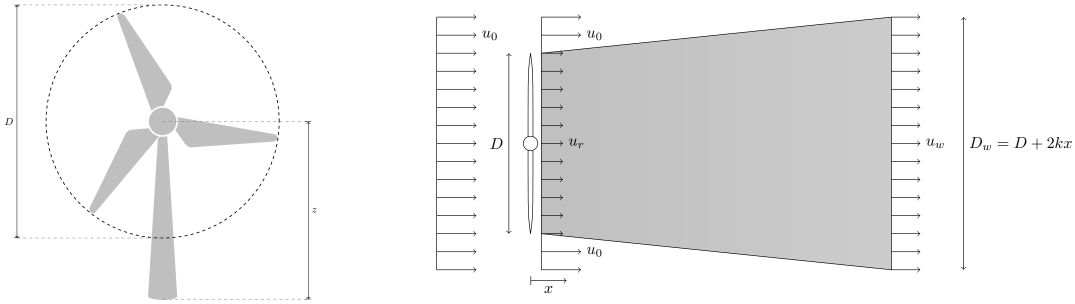

(a) Wind turbine (b) Generated wake

Figure 4.: Wind turbine with hub height z and rotor diameter D. The wake diameter D_w grows linearly by $2k$. Inside the wake, the incident wind speed u_0 is reduced to the wake velocity u_w. The Figures are taken from Heiming (2015).

To compute the incident velocity of a wind turbine, we simply use a weighting factor β between the free stream velocity u_0 and the wake velocity $u_w(x)$, which is computed by the circular intersection $A_{\text{Intersection}}$ of the wake cross section with the turbine's circular area A_{Turbine}, $\beta = \frac{A_{\text{Intersection}}}{A_{\text{Turbine}}}$.

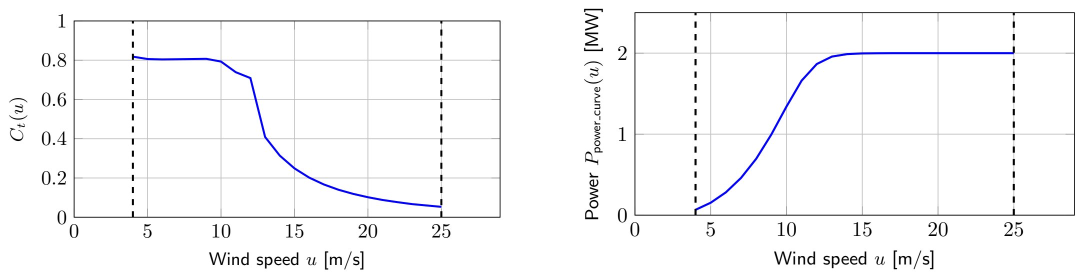

Figure 5.: Thrust coefficient C_t and power production of the turbine Vestas V80 with cut-in speed of 4 m/s and cut-out speed of 25 m/s (dashed vertical lines).

2.3. *Power Generation Model*

Turbines convert the wind's kinetic energy into electrical energy. Thus, the generated power of a wind turbine P depends on the incident wind speed u and the power curve (which is usually provided by the manufacturer as seen in Figure 5),

$$P(u) = P_{\text{power\_curve}}(u) \cdot \ell_{\text{power}}. \tag{3}$$

With the parameter ℓ_{power}, power curve losses are considered, such as material performance deviations from the expected power curve. The power curve depends on a cut-in speed u_{cutin} and a cut-out speed u_{cutout} which specify the range of wind speeds in which the turbine generates power. If the wind speed is lower than u_{cutin} there is not enough wind for efficient power production, and for wind speeds larger than u_{cutout} the wind is too strong such that the turbine might be damaged.

The gross annual energy production is given as the produced power for the duration of one year (in hours), thus

$$E_{\text{AEPgross}} = (8760h + 6h) \cdot P, \tag{4}$$

while the total generated power P is computed from the generated power for each wind direction φ,

$$P := \int_0^{2\pi} P_\varphi d\varphi \approx \sum_{i=1}^{N_{\text{dir}}} w_{\varphi_i} \cdot P_{\varphi_i}, \tag{5}$$

with direction φ_i, weight w_{φ_i} of the quadrature rule. The power P_{φ_i} for one wind direction is given by integrating along the corresponding probability function and the power curve.

2.4. *Cost Model*

As a result of the last three sub-models we can compute a value for the gross annual energy production by integrating for each wind direction and wind speed, computing the wake velocity for subsequent turbines and evaluating the power curve (see Figure 1). This value is now used to compute different economic indicator functions, e.g. the annual energy production, the levelized cost of electricity by Lackner and Elkinton (2007), the net present value by González, Rodríguez, Mora, Santos, and Payán (2009), or the internal rate of return by Çakar (2017). In this work, we consider the following two economic indicator functions:

- The *annual energy production*,

$$E_{\text{AEP}} = E_{\text{AEPgross}} \cdot \ell_{\text{performance}}, \tag{6}$$

is the basic quantity for most economic indicator functions. With the plant performance loss $\ell_{\text{performance}}$, we consider electrical losses due to availability of turbines, high wind hysteresis, and environmental performance degradation, such as icing and high temperatures.

- The *levelized cost of electricity* given by Lackner and Elkinton (2007)

$$K_{\text{LCOE}} = \frac{C_{\text{capital}} \cdot \dfrac{(1+r_{\text{rate}})^T \cdot r_{\text{rate}}}{(1+r_{\text{rate}})^T - 1} + C_{\text{O\&M}}}{E_{\text{AEP}}}, \tag{7}$$

with total installed capital costs C_{capital} for turbines, cabling, substation, decommission etc., annual operation and maintenance costs $C_{\text{O\&M}}$, and discount rate r_{rate} including debt, taxes, and insurance over the time period T.

2.5. *Validation of the Model*

The implemented model was cross-validated using the Openwind software, see Brower and Robinson (2012).

3. Stochastic Model for the Annual Energy Production in Wind Farms

The models described in Section 2 are purely deterministic, i.e. they will always compute the same results given the same input parameter. But to consider disturbances in some parameters we need to introduce some random variables and include them in the model to finally get a stochastic model.

3.1. *Uncertain Parameters*

The deterministic model from Section 2 is extended considering uncertainties in the parameters. In DNV (2013) several uncertainty–inflicted parameters at high level have been identified, listed in Table 1. The input parameters are now modeled as random variables ξ_i to consider the uncertain disturbance on them. In this work we are modeling all random variables as independent and normally distributed $\xi_i \sim \mathcal{N}(\mu_i, \sigma_i)$, whose mean is centered around the original undisturbed value μ_i. We want to stress, that this is a modeling assumption and might not be suitable for some of the presented uncertainties. As most of the modeled random variables originate from measurement data, a normal distribution should provide a good approximation of the actual distribution. For parameters with mathematical thresholds (e.g. the ξ_{ct} random variable in equation 9), where the unbounded support of the normal distribution can lead to problems, we instead use a truncated normal distribution. See Table 1 for a complete list of all random variables and their associated distributions. Choosing normal distributions also yields benefits for the analysis of a high dimensional joint probability distribution function in the case studies presented in section 5. The economically-based random variables are almost surely independent from the ones from the physical models and are also independent from each other as they all address separate topics. The same holds for most of the uncertain variables from the physical domain. The uncertainty in the thrust coefficient C_t for example is considered to be a geometric design property of the turbine blades and thus the uncertainty lies within the generated thrust and not the static pressure on the blades. This also holds for the power curve where the uncertainty is modeled in the mapping of the wind velocity to the produced power and thus is independent from the velocity itself. Recently, the effect of lift coefficients on the performance of wind turbine blades was emphasized as a factor contributing to uncertainty. This influences the estimation of the power curve and can increase uncertainty sources, see Li and Caracoglia (2020). Thus, for the independence of uncertain parameters we only assume the independence of the uncertainty on the surface roughness and the uncertainty in the measured wind speed.

Each random variable can be rewritten to a multiplication between the undisturbed value and a normal distribution $\mathcal{N}(1, \sigma)$ with the mean value of one. As the standard deviation σ is a relative property, it can be chosen to resemble any observed deviation d. In this work, the deviation of the measurement data d describes the exceedance probability of 90% and therefore σ can be computed by evaluating the inverse of its distribution function for which, in case of the normal distribution, 90% of the data lies below the bell curve. The following uncertain parameters are considered:

- *Wind speed*, due to site measurements, historic wind resource or the measure-correlate-predict method, vertical extrapolation, future variability, and wind flow extrapolation.
- *Wake effect*, due to model inaccuracies and neighboring sites.
- *C_t curve*, due to impacts of atmospheric stability and site conditions for which C_t curve is not valid.
- *Surface roughness*, due to changing surface conditions caused by weather or tides.
- *Power curve*, due to impacts of atmospheric stability, and site conditions for which power curve is not valid.
- *Plant performance*, due to electrical efficiency, availability of turbines, internal and external grid, due to environmental as blade soiling, blade degradation and weather effects.
- *Capital costs*, due to steel price fluctuations.
- *Annual O&M costs*, due to use of new technologies.
- *Discount rate*, due to fluctuations of the economic discount rate.

Uncertain parameters		Distribution
Wind speed	ξ_{wind}	Normal
Wake effect	ξ_{wake}	Normal
C_t curve	ξ_{ct}	truncated Normal
Surface roughness	ξ_{rough}	truncated Normal
Power curve	ξ_{power}	Normal
Plant performance	$\xi_{\text{performance}}$	Normal
Capital costs	ξ_{capital}	Normal
Annual O&M costs	$\xi_{\text{o\&m}}$	Normal
Discount rate	ξ_{rate}	Normal

Table 1.: Uncertain parameters of the wind farm model at high level.

3.2. *Stochastic Model*

The above defined random variables are now included into the model to finally get a stochastic model.

Wind Due to inaccurate measurements, imprecise long-term predictions, inter-annual variability, and further interference DNV (2013), the distribution of the wind speed u is a highly uncertain parameter. Therefore, we disturb the raw data of the wind speed with a normally distributed random variable ξ_{wind} such that disturbed probability density functions of the Weibull distribution are obtained (see Figure 6). In Çakar (2017) and in Tuzuner and Yu (2008) it is shown that a disturbance d of the wind speed corresponds to the disturbance d of the Weibull parameter λ, such that the resulting probability for each wind speed u can be formulated as a random variable. Compare with equation (1):

$$\mathcal{W}(u; \lambda, k, \xi_{\text{wind}}) = \left(\frac{k}{\lambda \cdot \xi_{\text{wind}}} \right) \cdot \left(\frac{u}{\lambda \cdot \xi_{\text{wind}}} \right)^{k-1} \cdot \exp\left(-(u \cdot \lambda \cdot \xi_{\text{wind}})^k \right), \tag{8}$$

where $\lambda > 0$ is the scale parameter and $k > 0$ is the shape parameter of the Weibull distribution, which are determined with the maximum likelihood estimation using the undisturbed wind speed data.

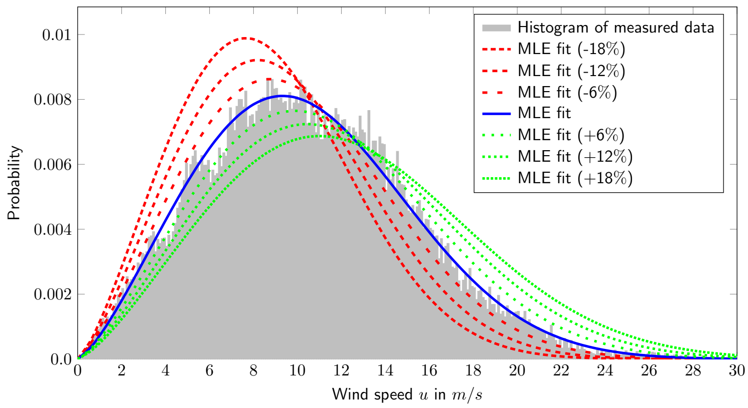

Figure 6.: Fitted Weibull distribution with maximum likelihood estimation (MLE) for the wind speed distribution over the years from January 2010 to December 2017 for the western wind direction sector (255° to 285°) measured at the FINO3 research platform. Red and green plots represent the fitted Weibull distribution with MLE after disturbing the wind speed data with factors of ±6%, ±12%, and ±18%. The random variable $\xi_{wind}(u)$ represents the Weibull distribution between the highest red plot (MLE fit -18%) and the lowest green plot (MLE fit +18%) with a probability of 99.73%.

Wake Within a wind farm or outside of the wind farm there can be some wake effects from future installations. The predicted wake effect is disturbed due to uncertainty in the model inputs (including wind direction), model performance, and appropriateness for the site. Furthermore we need to include uncertainty related to any proposed neighboring sites (construction time, layout, turbine type), see DNV (2013). Therefore we disturb the velocity deficit of a wake with a normally distributed random variable ξ_{wake}. Furthermore, the wake model depends on the C_t curve and the surface roughness z_0. Due to imprecise measurements of the C_t curve, we disturb this parameter with the random variable ξ_{ct} (see Figure 7). Here, in order to prevent negative values in the root of the numerator of equation 9, we used a truncated normal distribution, which enforces $C_t(u_0) \cdot \xi_{\text{ct}} \leq 1$ as this could otherwise lead to non-physical complex wake velocities.

The surface roughness depends on the topography and flora, see Wierngа (1993), i.e. for offshore wind farms it depends on the wave field, wind speed, upstream fetch, and water depth, see Lange, Larsen, Højstrup, and Barthelmie (2004). Thus, also this parameter z_0 should be stochastic and is therefore disturbed with a truncated normally distributed random variable ξ_{rough} to enforce $z_0 \cdot \xi_{\text{rough}} > 0$. Altogether, the wind speed behind a turbine at any point x from equation (2) changes as follows:

$$\widetilde{u_w}\big(x, \xi_{\text{wake}}, \xi_{\text{ct}}, \xi_{\text{rough}}\big) = (\ell_{\text{wind}} \cdot u_0) - \frac{1 - \sqrt{1 - C_t(\ell_{\text{wind}} \cdot u_0) \cdot \xi_{\text{ct}}}}{\big(1 + \frac{2x}{D} \cdot \frac{1}{2\ln(z/(z_0 \cdot \xi_{\text{rough}}))}\big)^2} \cdot \ell_{\text{wake}} \cdot \xi_{\text{wake}} \cdot (\ell_{\text{wind}} \cdot u_0). \tag{9}$$

Power generation In the power generation model the turbine performance is disturbed due to material fatigue which leads to uncertainty in the power curve. Furthermore, there is uncertainty in performance under site conditions for which the power curve is not valid. This also includes the impact of atmospheric stability and uncertainty associated with uncertain icing losses as well as other environmental losses, e.g. blade soiling, blade degradation, weather effects. As it is difficult to quantify these sources of uncertainty in terms of individual standard deviations, we model them as a single uncertain parameter and thus disturb the power curve by the normally distributed random variable ξ_{power} (see Figure 7). This changes equation (3) for the power curve as follows:

$$\widetilde{P}(u, \xi_{\text{power}}) = P_{\text{power\_curve}}(u) \cdot \ell_{\text{power}} \cdot \xi_{\text{power}}. \tag{10}$$

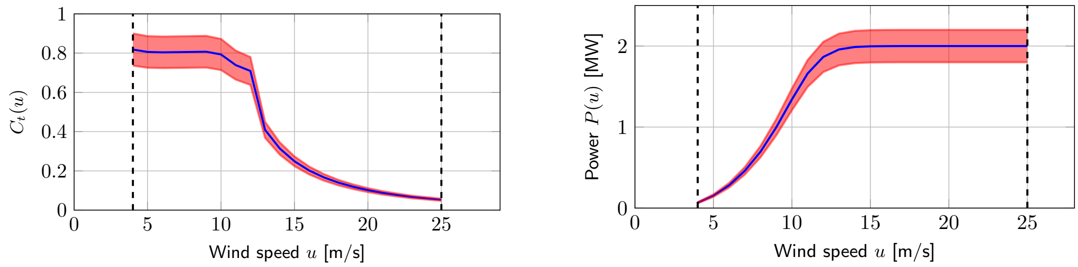

Figure 7.: Exemplary disturbed C_t and power curve of a Vestas V80 turbine with a cut-in speed of 4 m/s and cut-out speed of 25 m/s (dashed vertical lines). The red tube illustrates the C_t and power curve with a disturbance of $\pm 10\%$.

Annual energy production The *annual energy production* is the basic value for all other economic indicator functions. As plant performance losses due to e.g. availability or curtailment are uncertain, we disturb the performance with the normally distributed random variable $\xi_{\text{performance}}$, which results into the following formula:

$$\widetilde{E}_{\text{AEP}} = E_{\text{AEPgross}} \cdot \ell_{\text{performance}} \cdot \xi_{\text{performance}}. \tag{11}$$

Levelized cost of electricity The capital costs C_{capital} mainly depend on the price of steel. But because of the long planning stage of several years for a wind farm, the calculation depends on long-term predictions for the steel price which is very volatile. Therefore, we disturb the capital costs with a normally distributed random variable ξ_{capital}. The same argument holds for the discount rate r_{rate}, which during an early planning stage is very tentative thus it is disturbed with a normally distributed random variable ξ_{rate}. The costs for annual operation and maintenance $C_{\text{O\&M}}$ are also affected by the volatile price of steel (for the material), and other political decisions like payroll taxes. Therefore, this parameter is also disturbed with a normally distributed random variable $\xi_{\text{o\&m}}$. Altogether, the the levelized cost of electricity from (7) changes as follows:

$$\widetilde{K}_{\mathrm{LCOE}} = \frac{C_{\mathrm{capital}} \cdot \xi_{\mathrm{capital}} \cdot \dfrac{(1+\tilde{r}_{\mathrm{rate}})^T \cdot \tilde{r}_{\mathrm{rate}}}{(1+\tilde{r}_{\mathrm{rate}})^T - 1} + C_{\mathrm{O\&M}} \cdot \xi_{\mathrm{o\&m}}}{\widetilde{E}_{\mathrm{AEP}}}, \tag{12}$$

with disturbed discount rate $\tilde{r}_{\mathrm{rate}} = r_{\mathrm{rate}} \cdot \xi_{\mathrm{rate}}$.

4. Methods of Uncertainty Quantification

As is it the goal of this paper to investigate the influence of uncertainties in the input parameters onto different model outputs, e.g. gross annual energy production, it is necessary to introduce methods which allow quantifying their influence on a certain quantity of interest. The overall idea of propagating uncertainties through models and then computing the sensitivities of these models in relation to the inputs is in literature referred to as Uncertainty Quantification (UQ).

From a practical point of view the methods for Uncertainty Quantification, see Smith (2013), Sullivan (2015), de Cursi and Sampaio (2015), Ghanem, Higdon, and Owhadi (2017), can be divided into two different categories: While *intrusive* methods introduce changes to the original problem as the governing equations become statistical, *non-intrusive* methods on the other hand evaluate the original problem with varying inputs and compute the statistics from the results. For complex problems, a non-intrusive method is often favored as it requires no modification to the original code. While Lackner and Elkinton (2007) and Foti et al. (2017) used a Monte Carlo simulation, Murcia et al. (2015) performed a Latin Hypercube simulation for their investigations.

In this paper the influence of the uncertainty of some parameters in the context of an offshore wind farm will be investigated by the means of the classical Monte Carlo method, see Smith (2013), low-discrepancy quasi-Monte Carlo methods by Niederreiter (1992), and also the Stochastic Collocation method by Babuška, Nobile, and Tempone (2007). We will then provide a recommendation for the method which performs best with respect to the underlying offshore wind farm problem setting.

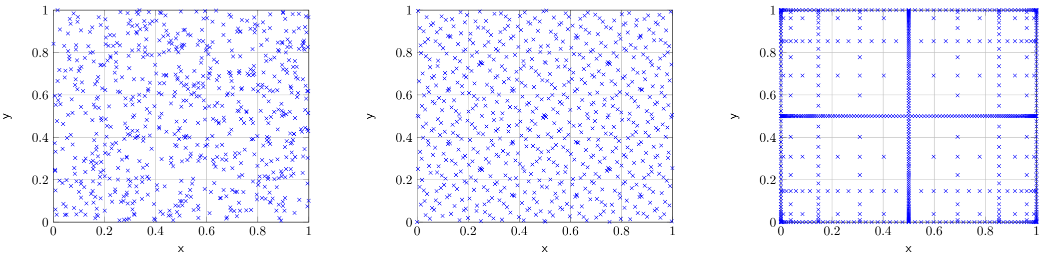

(a) Monte Carlo (b) Quasi-Monte Carlo (c) Stochastic Collocation on sparse grids

Figure 8.: Visual representation of different sampling strategies on a two-dimensional unit square. (a) classical Monte Carlo with pseudo random numbers generated by the Mersenne Twister Engine from the C++ standard library, (b) Quasi-Monte Carlo with pseudo random numbers generated by the Sobol sequence, and (c) Stochastic Collocation on Smolyak sparse grids with Clenshaw Curtis nodes.

4.1. *Monte Carlo*

In order to compute a given quantity of interest, such as the expectation of the annual energy production, the problem can be written mathematically as:

$$\mathbb{E}[u(\vec{X},\vec{\xi})] = \int_{\Gamma} u(\vec{X},\vec{\xi})\rho(\vec{\xi})d\vec{\xi}, \tag{13}$$

where $u(\vec{X},\vec{\xi})$ is the disturbed model involved in computing the annual energy production, $\vec{\xi}$ are the random variables modeling uncertainties within the inputs, $\rho(\vec{\xi})$ as the respective probability density function, and $\vec{X}$ the vector of undisturbed parameters. The Monte Carlo method uses sampling in the probability space of the associated random variable $\vec{\xi}$ to evaluate the integral in equation 13. By computing M deterministic solutions (sampling), each starting from a different set of realizations of the uncertain parameters, M solutions of the type $u^m(\vec{X}) = u(\vec{X},\vec{\xi}^m)$ are obtained. If $\vec{\xi}^m$, $m = 1,\ldots,M$ is a sequence of independent and identically distributed random variables, application of the central limit theorem yields:

$$\frac{1}{M}\sum_{m=1}^{M} u(\vec{X},\vec{\xi}^m) \xrightarrow{a.s.} \mathbb{E}[u(\vec{X},\vec{\xi})].$$

This means that, in the limit, the method converges to a fixed value for the mean and also the variance of the Quantity of Interest. The rate of convergence for the Monte

Carlo method with random sampling is $\mathcal{O}(M^{-1/2})$, as shown by Caflisch (1998). $\mathcal{O}(\cdot)$ in this context describes the upper bound for the growth rate of a function. Therefore, in order to achieve one additional digit of accuracy, it is necessary to compute 100 times more samples. This slow convergence rate can cause issues in case of computationally expensive problems. On the other hand, the convergence rate of the Monte Carlo sampling is not a function of the dimension of the probability space.

Generating random numbers for the sampling process is a difficult task in practice as computers are deterministic machines. In this work we use pseudo random numbers generated by the Mersenne Twister method by Matsumoto and Nishimura (1998) from the C++ standard library. A visual representation of generated samples can be seen in Figure 8a.

4.2. *Quasi-Monte Carlo*

An improvement to the classical Monte Carlo method is the quasi-Monte Carlo method (QMC). It relies on the sample principle like the classical Monte Carlo method with the difference being, that it makes use of a low-discrepancy sequence in order to generate its random numbers. Morokoff and Caflisch (1995) examined three different low discrepancy sequences: the Halton, Sobol, and Faure sequence. The result indicated that Halton sequences are best for up to six dimensions and the Sobol sequence is best for all higher dimensions. As we are interested in these high dimensional cases, the Sobol sequence is used in this paper. The Sobol sequence can be briefly explained as a sequential instruction set that fills a multi-dimensional hypercube, while trying to avoid the creation of void regions. These created values are deterministic and thus are called pseudo-random, but they evenly fill the hypercube and therefore potentially lead to a faster convergence compared to the pure Monte-Carlo method. The more equal filling can be seen in Figure 8b. For a detailed explanation regarding the generation of the sequence, see Bratley and Fox (1988). By using the Sobol sequence to generate pseudo random numbers, the convergence of the quasi-Monte Carlo is of the order $\mathcal{O}(M^{-1}(\log M)^{\dim(\vec{\xi})})$, see Caflisch (1998). This means that for small dimensions, the quasi-Monte Carlo simulation only needs to compute roughly five to ten times fewer samples in order to achieve one additional digit of accuracy compared to the classical

Monte Carlo method.

4.3. *Sparse Grid Stochastic Collocation*

Compared to the previous methods, the sparse grid Stochastic Collocation (SC) method is not a variant of the classical Monte Carlo method. The main idea of the sparse grid Stochastic Collocation method is to choose a set of M collocations points in probability space and then to compute the solution at these points. As the positions of the collocation points are generally freely chosen, the sparse grid Stochastic Collocation method selects them based on a quadrature rule and exploits the corresponding quadrature weights to compute the statistics of a given quantity of interest such as e.g. the annual energy production. In case of a high dimensional probability space it is thus necessary to use an efficient quadrature rule, as for common methods the number of required quadrature points increases exponentially with the dimension of the probability space. This leads to overall expensive computations as a solution of the deterministic problem needs to be computed on every quadrature point.

One way to construct such an efficient rule is by using the so-called Smolyak sparse grids. These grids are constructed from nested one-dimensional quadrature rules, which restricts the degrees of freedom involved in the discretization of the problem and thus allows for a slower growth of the required quadrature points. In this paper Smolyak sparse grids with Clenshaw Curtis nodes are used for the computations involving the sparse grid Stochastic Collocation method. As this node type yields a quadrature set for the bounded interval $[-1, 1]$ and thus would not be a suitable quadrature rule for unbounded probability density functions as e.g. the normal distribution, we use an inverse cumulative distribution function transform to expand the quadrature set to $(-\infty, \infty)$ as described in van Wyk, Gunzburger, and Burkardt (2016). For further details on the sparse grid method, see Smith (2013); Wolters (2016). Figure 8c shows an example for such a sparse grid for the domain $[0, 1]^2$.

The convergence rate of the method is of the order $\mathcal{O}(M^{-\alpha}(\log M)^{(\dim(\vec{\xi})-1)(\alpha+1)})$, with dimension of the uncertain parameter space d, M as total number of grid points and α depending on the regularity of the solution. It has to be stressed that the number of samples M is indirectly determined by the dimensionality of the probability space and the level of the underlying quadrature rule which can be selected by the user. Also differing from the previously discussed Monte Carlo type methods, is the convergence rate of the sparse grid Stochastic Collocation method as it decreases for higher dimensions. This phenomenon is often referred to as the “curse of dimensionality” and restricts usability of collocation methods for high dimensional probability spaces.

4.4. ***Error Comparison of UQ Methods***

In order to demonstrate the convergence behavior of the described methods, we use the computation of the levelized cost of electricity (see Figure 1) as a benchmark. The uncertain parameters in this computation resemble the maximal amount of parameters in the results presented in Section 5. The associated probability distributions used in the sampling process for each parameter can be seen in Table 4, while the remaining input data is configured according to the *Horns Rev 1* wind farm dataset. As we are computing the levelized cost of electricity, all nine parameters from Table 4 have an influence on the solution and therefore the resulting joint probability space is nine-dimensional.

The convergence rates of all presented methods are recapitulated in Table 2. As these

Monte Carlo	quasi-Monte Carlo	Sparse Grid Stochastic Collocation
$\mathcal{O}(M^{-1/2})$	$\mathcal{O}(M^{-1}(\log M)^{\dim(\vec{\xi})})$	$\mathcal{O}(M^{-\alpha}(\log M)^{(\dim(\vec{\xi})-1)(\alpha+1)})$

Table 2.: Order of the convergence rates of the presented UQ methods.

values only show the theoretical order and neglect the influence of any constant factors, Figures 9 and 10 show the numerically studied error evolution patterns. This is especially interesting for the sparse grid Stochastic Collocation method, as its convergence rate depends on the unknown smoothness α of the underlying problem. The methods are compared in terms of the relative error in the expectation and variance with respect to a quasi-Monte Carlo simulation computed with a sufficiently large sample size of $M = 1 \cdot 10^8$. Normally the classical Monte Carlo simulation should be used as a reference as it will always converge towards the correct result for $M \to \infty$, but the high dimensionality of the problem combined with the slow convergence rate of the method demanded an unreasonable sample size.

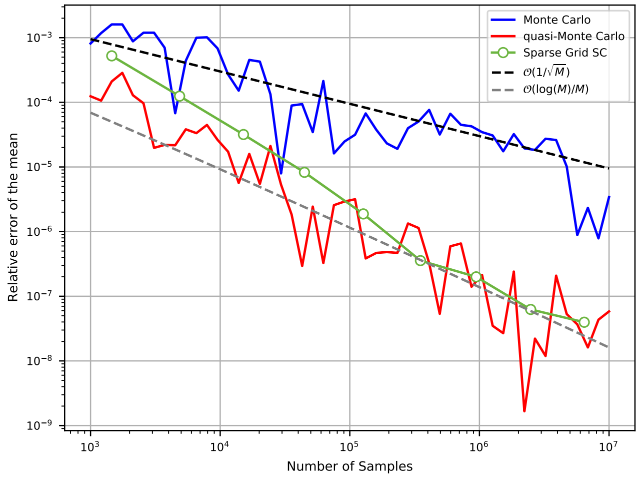

Figure 9.: Convergence behavior of the presented methods in terms of the relative error in the mean w.r.t to the quasi-Monte Carlo reference solution.

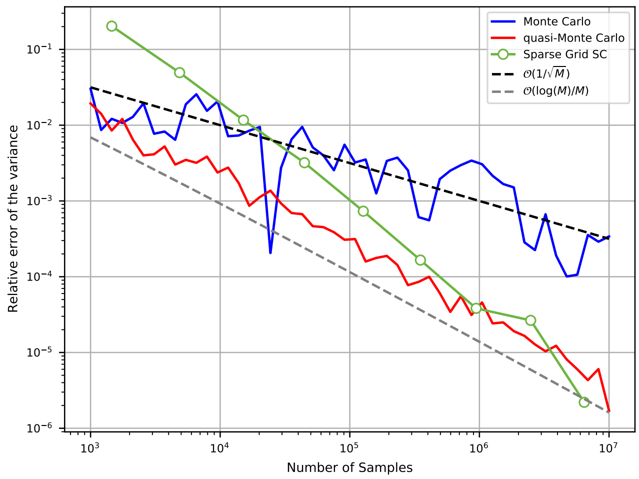

Figure 10.: Convergence behavior of the presented methods in terms of the relative error in the variance w.r.t to the quasi-Monte Carlo reference solution.

The presented results show that the Monte Carlo is the least accurate method in terms of the observed relative error across all sample sizes which coincides with its theoretical convergence rate. The sparse grid Stochastic Collocation method shows a higher convergence rate compared to the quasi-Monte Carlo method, despite having a higher initial error for lower grid levels. Both methods achieve similar relative errors of $7 \cdot 10^{-7}$ for the expectation and $9 \cdot 10^{-5}$ for the variance with respect to the reference quasi-Monte Carlo solution. The dashed lines in Figure 9 and 10 show the theoretical convergence rates of the classical Monte Carlo and the quasi-Monte Carlo methods. While the classical Monte Carlo method shows the expected convergence rate, it is worth noting that the quasi-Monte Carlo method, whose convergence rate is plotted with $\dim \vec{\xi} = 1$, shows a comparable error decline despite the much higher dimensionality of the problem. This implies that the probability space of the underlying problem might be dominated by a single dimension and that the low discrepancy sequence of the method can successfully exploit this fact for an accelerated convergence behavior. This observation becomes more apparent in the sensitivity analysis presented in Section 5.

Considering the computational costs of both methods, the costs of computing the sparse grid for the Stochastic Collocation method scale in a nonlinear way with the dimension of the probability space and the grid level, while the sequence generation of the quasi-Monte Carlo method is linear in the number of sample points and thus potentially faster for large numbers of samples/dimensions. As the grid calculations could also be done once and stored prior to the actual Uncertainty Quantification analysis, this does not pose a significant drawback except for very high dimensions and many grid levels.

Based on the obtained results, it can be concluded that the quasi-Monte Carlo method is favorable over the other methods. This observation is based on the three criteria: error control, computational overhead, and finally ease of implementation. While Stochastic Collocation and quasi-Monte Carlo yield comparable results for the demonstrated sample sizes, it has to be stressed that the reference solution has also been computed using quasi-Monte Carlo method and the relative error thus has a bias in favor of quasi-Monte Carlo. Purely based on the observed relative convergence rate, the Stochastic Collocation method converges at a higher rate. Quasi-Monte Carlo allows for an arbitrary sample size and thus a fine-grained error control, while the used sparse grids in the Stochastic Collocation method, only allows for very discrete sample sizes, which exponentially increase with the selected level (see marker in the Stochastic Collocation plots in Figures 9 and 10) due to the inherent nestedness of quadrature nodes. Furthermore, quasi-Monte Carlo does not required any precomputations, as computing the next sample from the Sobol sequence has negligible computational

cost. Lastly, numerical codes for the Sobol sequence have better availability across multiple programming languages compared to arbitrary dimension and level sparse grid generators.
The presented results in Section 5 are therefore solely obtained by the application of the quasi-Monte Carlo method. For the sample size we choose $1 \cdot 10^6$ samples as the obtained results show a relative error of $\mathcal{O}(10^{-6})$ for the LCOE, which also includes the computation of the AEP (see Figure 1) and thus errors for the mean should be of the order $\mathcal{O}(1)$ [GWh] for all presented test cases.

5. Case Study Results

This section describes the evaluation of the stochastic models introduced in Section 3 by using the methods of Uncertainty Quantification from Section 4. The influence of the input variables on the computed annual energy production and levelized cost of electricity will be determined, and their computed statistics will be analyzed.

For the model we will use the parameters of the three wind farms *Horns Rev 1*[1], *DanTysk*[2], and *Sandbank*[3]. As each of these wind farms differ significantly in the used turbine types and grid layout, they will also have different losses and sensitivities with respect to the presented uncertainties. Because the wind farms are all closely positioned on a global scale, the same wind data will be used in each of the evaluations. The source of this wind data is the FINO3[4] met mast, positioned about 50 km southwest of Horns Rev, 2 km west from DanTysk, and 20 km east from Sandbank. We use all data recorded between January 2010 and December 2017 at a height of 100 meters.

For each wind farm, turbine positions are given in Figure 11, its turbine C_t and power curves are shown in Figure 12, while its general settings, losses, and uncertainties are listed in Tables 3 and 4. The values presented in these tables originate from data which was gathered over multiple years by the Vattenfall Europe Windkraft GmbH.

Before analyzing the propagation of uncertainties, we introduce some of the notation used by the variance-based sensitivity analysis for the joint probability space,

[1] More information: `https://powerplants.vattenfall.com/horns-rev`
[2] `https://powerplants.vattenfall.com/dantysk`
[3] `https://powerplants.vattenfall.com/sandbank`
[4] `https://www.fino3.de/en/`

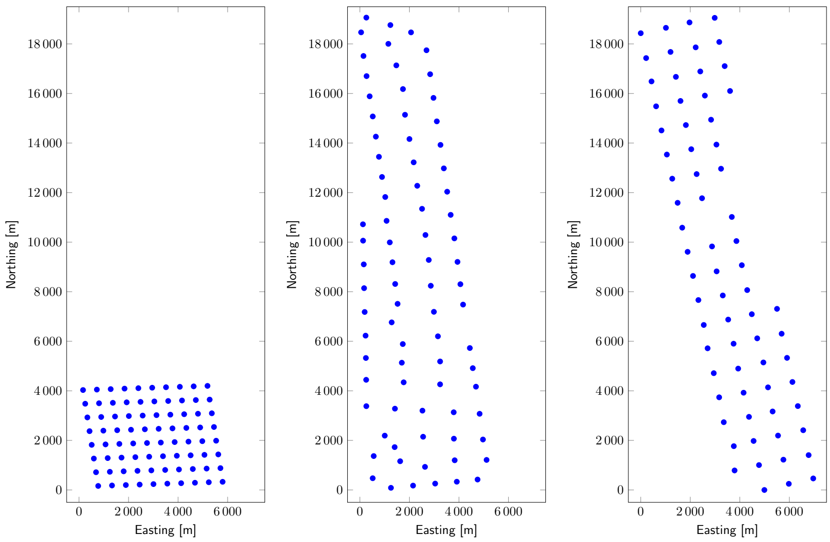

Figure 11.: Turbine positions for the wind farms Horns Rev 1 (left), DanTysk (center), and Sandbank (right). The constructed wind farm *Horns Rev 1* is located in the North Sea close to the Danish coast. This wind farm has been built in 2002 and is commonly used as a test case for all kinds of offshore wind farm related research, e.g. Murcia et al. (2015), Gaumond et al. (2014), Barthelmie et al. (2009). The *DanTysk* wind farm is located close to the German shore in the North Sea, approximately 70 km west of the island Sylt. Build in 2014, it covers an area of 70 square meters and can theoretically produce 288 MW of power, if each of its 80 turbines would operate at full load. The *Sandbank* wind farm is located right next to the DanTysk wind farm and is the newest of all presented wind farms as it was recently built in 2017. Containing 72 turbines, laid out in rows across an area of 60 square kilometers, each capable of producing 4 MW of electrical power, the wind farm has a theoretical peak electrical power output of 288 MW. The turbines also have a much higher cut-out speed compared to the turbines of the other two wind farms.

spanned by the uncertainties w.r.t. all nine variables given in Table 1, as described by Saltelli et al. (2010). This notation is especially designed to express how the uncertainty in the model output can be linked to uncertainties in the inputs. The stochastic model derived previously will be represented by Y in the following, while the model inputs will be referred to as ξ_i. The uncertainty propagation of ξ_i through Y is best described in the context of this notation by the sensitivity measure by Saltelli et al. (2010)

$$S_i = \frac{\mathrm{var}_{\xi_i}(E_{\xi_{\sim i}}(\mathrm{Y}|\xi_i))}{\mathrm{var}(\mathrm{Y})}, \tag{14}$$

which is technically the first order sensitivity coefficient that measures e.g. the additive

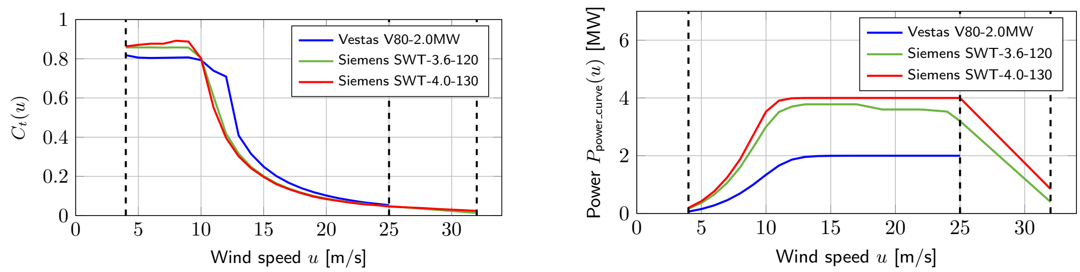

Figure 12.: Thrust coefficient C_t (left) and power production (right) of the turbines Vestas V80 by L. Jensen et al. (2004), Siemens SWT-3.6-120, and Siemens SWT-4.0-130. The dashed vertical lines show the cut-in and cut-out speeds.

Parameter		Horns Rev 1	DanTysk	Sandbank
Positions		see Figure 11	see Figure 11	see Figure 11
Wind data		FINO3 (2010–2017)	FINO3 (2010–2017)	FINO3 (2010–2017)
Wind speed losses	ℓ_{wind}	98.5 %	99.2 %	99.5 %
Turbine type		Vestas V80-2.0MW	Siemens SWT-3.6-120	Siemens SWT-4.0-130
Rotor diameter	D	80 m	120 m	130 m
Hub height	z	70 m	88 m	95 m
Cut-in speed	u_{cutin}	4 m/s	4 m/s	4 m/s
Cut-out speed	u_{cutout}	25 m/s	32 m/s	32 m/s
Surface roughness	z_0	$0.2 \cdot 10^{-3}$ m	$0.2 \cdot 10^{-3}$ m	$0.2 \cdot 10^{-3}$ m
Wake effect losses	ℓ_{wake}	99.9 %	99.9 %	99.9 %
Power curve	$P(u)$	see Figure 12	see Figure 12	see Figure 12
C_t curve	$C_t(u)$	see Figure 12	see Figure 12	see Figure 12
Power curve losses	ℓ_{power}	98.8 %	98.9 %	99 %
Total capital costs	C_{capital}	278 000 000 €	1 000 000 000 €	1 200 000 000 €
Annual operation and maintenance costs	$C_{\text{O\&M}}$	52 000 000 €	43 200 000 €	43 200 000 €
Discount rate	r_{rate}	2 %	3.75 %	0.15 %
Project lifetime	T	20 years	20 years	20 years
Plant performance losses	$\ell_{\text{performance}}$	88.5 %	88.8 %	89 %

Table 3.: Parameters for the wind farms Horns Rev 1, DanTysk, and Sandbank.

effect of ξ_i on the model output. S_i can also be interpreted in terms of expected reduction of variance. This interpretation allows an easier understanding of the factors involved in the computation of S_i:

- var(Y): output variance with all inputs modeled as random variables
- $\text{var}_{\xi_i}(E_{\xi_{\sim i}}(\text{Y}|\xi_i))$: expected reduction in variance that would be obtained if ξ_i could be fixed

In the following we use box plots to visualize statistical characteristics of the solution. The inside of the box, bounded by the lower and upper quartiles, represents 50 % of the computed samples. The vertical line inside the box stands for the median of the data set. The lower whisker is the smallest data value which is larger than: lower quartile − 1.5 · inter-quartile-range, where the "inter–quartile–range" is the difference between the upper and lower quartiles. The upper whisker is the largest data value which is

Uncertainty		Horns Rev 1		DanTysk		Sandbank	
		deviation	σ	deviation	σ	deviation	σ
Wind speed	ξ_{wind}	8.0%	0.0486	6.0%	0.0365	7.5%	0.0456
Wake effect	ξ_{wake}	3.0%	0.0182	3.0%	0.0182	3.0%	0.0182
C_t curve	ξ_{ct}	2.0%	0.0122	2.0%	0.0122	2.0%	0.0122
Surface roughness	ξ_{rough}	0.000021%	$1.277 \cdot 10^{-7}$	0.000017%	$1.034 \cdot 10^{-7}$	0.000016%	$9.737 \cdot 10^{-8}$
Power curve	ξ_{power}	2.0%	0.0122	2.0%	0.0122	2.0%	0.0122
Plant performance	$\xi_{\text{performance}}$	2.3%	0.0140	2.1%	0.0128	2.1%	0.0128
Capital costs	ξ_{capital}	3.0%	0.0182	3.0%	0.0182	3.0%	0.0182
Annual O&M costs	$\xi_{\text{o\&m}}$	3.0%	0.0182	3.0%	0.0182	3.0%	0.0182
Discount rate	ξ_{rate}	4.0%	0.0234	1.0%	0.0061	0.5%	0.0030

Table 4.: Uncertain parameters for the wind farms Horns Rev 1, DanTysk, and Sandbank. The surface roughness parameter is given by using the maximum approximation of Foti et al. (2017), $\sigma_{rough} = 1.5 \cdot 10^{-5}/z$. The values presented in this table originate from data which was gathered over multiple years by the Vattenfall Europe Windkraft GmbH.

smaller than: upper quartile + $1.5 \cdot$ inter-quartile-range.

5.1. *Annual Energy Production*

In Figure 13 the results regarding the annual energy production for all six influencing uncertainty parameters, i.e. wind speed, wake effect, C_t curve, surface roughness, power curve, and power loss are shown. For their deviation we choose two test cases: an *academic test case* for which we choose equal deviations of 5 % for all six uncertainty-inflicted parameters, while for the *realistic test case* we choose the deviations as given in Table 4 by the Vattenfall Europe Windkraft GmbH.

Each box plot represents the results of an uncertain parameter. The topmost box plot represents the model output for the case that the six uncertainties are disturbed at the same time. In the box plot it can be seen that the deviation from the expected annual energy production value behaves similarly in both directions of the AEP. The deviations of the wind speed, power curve, and plant performance have the largest impact on the annual energy production in comparison to all other uncertainties. This holds for the academic and realistic test case.

The results in terms of the variance-based sensitivity analysis are shown in Table 5 (academic test case) and Table 6 (realistic test case). In the realistic test case, for all three wind farms the sensitivity is higher than 84 %. The sensitivities of the power curve and plant performance follow with about 3 to 9 percent. All remaining uncertainties (wake effect, C_t curve, and surface roughness) are below 0.3 % and thus have a rather negligible influence on the variance of the model output.

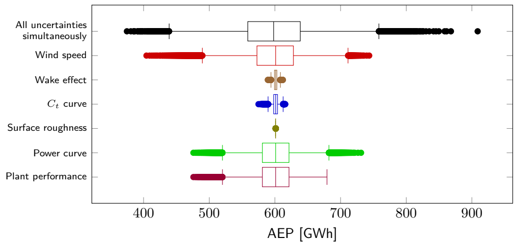

(a) Horns Rev 1 test case with equal deviations of 5 %.

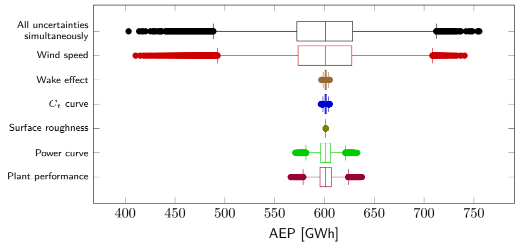

(b) Horns Rev 1 test case with different deviations according to Table 4.

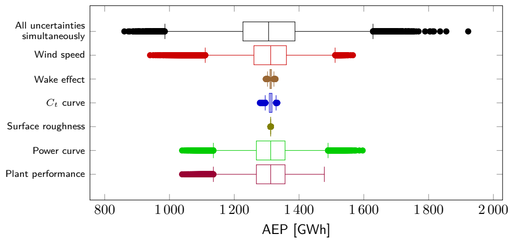

(c) DanTysk test case with equal deviations of 5 %.

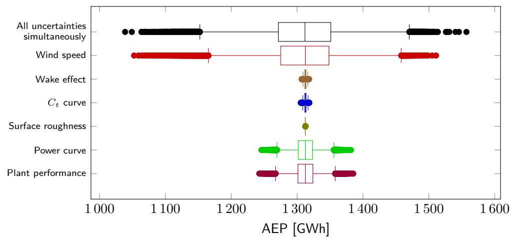

(d) DanTysk test case with different deviations according to Table 4.

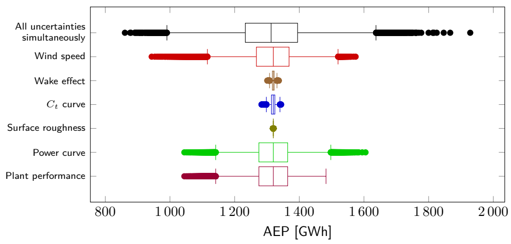

(e) Sandbank test case with equal deviations of 5 %.

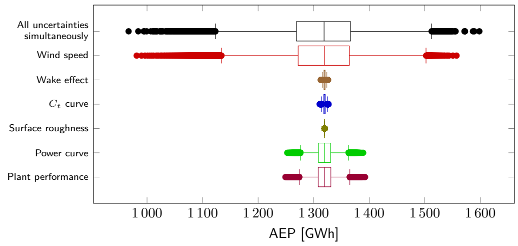

(f) Sandbank test case with different deviations according to Table 4.

Figure 13.: Graphical visualization of the sensitivity analysis with all six uncertainty parameters wind speed, wake effect, C_t curve, surface roughness, power curve, and plant performance at the same time (simultaneously) compared to single disturbances of the uncertainty parameters computed with the quasi-Monte Carlo method with 10^6 samples for the Horns Rev 1, DanTysk, and Sandbank wind farms. The mean AEP corresponds to the given values in literature, namely 599.5 GWh (Horns Rev 1), 1310.6 GWh (DanTysk), 1316.4 GWh (Sandbank).

Uncertainty		Horns Rev 1		DanTysk		Sandbank	
		variance	sensitivity	variance	sensitivity	variance	sensitivity
Wind speed	ξ_{wind}	$1.6887 \cdot 10^9$	48.12 %	$5.5619 \cdot 10^9$	39.3 %	$5.6467 \cdot 10^9$	39.36 %
Wake effect	ξ_{wake}	$1.1276 \cdot 10^7$	0.32 %	$3.125 \cdot 10^7$	0.22 %	$3.8256 \cdot 10^7$	0.27 %
C_t curve	ξ_{ct}	$2.1235 \cdot 10^7$	0.61 %	$5.1429 \cdot 10^7$	0.36 %	$7.266 \cdot 10^7$	0.51 %
Surface roughness	ξ_{rough}	$4.2003 \cdot 10^6$	0.12 %	$1.7947 \cdot 10^7$	0.13 %	$2.0629 \cdot 10^7$	0.14 %
Power curve	ξ_{power}	$9.0764 \cdot 10^8$	25.86 %	$4.3241 \cdot 10^9$	30.55 %	$4.3729 \cdot 10^9$	30.48 %
Plant performance	$\xi_{\text{performance}}$	$8.9968 \cdot 10^8$	25.63 %	$4.2771 \cdot 10^9$	30.22 %	$4.3179 \cdot 10^9$	30.1 %

Table 5.: Results of the variance-based sensitivity analysis where all uncertainties are fixed to 5 % of AEP calculation with 10^6 samples using the quasi-Monte Carlo Method.

Uncertainty		Horns Rev 1		DanTysk		Sandbank	
		variance	sensitivity	variance	sensitivity	variance	sensitivity
Wind speed	ξ_{wind}	$1.5966 \cdot 10^9$	92.81 %	$2.9557 \cdot 10^9$	84.61 %	$4.6948 \cdot 10^9$	89.7 %
Wake effect	ξ_{wake}	$3.6257 \cdot 10^6$	0.21 %	$5.7514 \cdot 10^6$	0.16 %	$1.2469 \cdot 10^7$	0.24 %
C_t curve	ξ_{ct}	$3.6569 \cdot 10^6$	0.21 %	$6.0823 \cdot 10^6$	0.17 %	$1.3101 \cdot 10^7$	0.25 %
Surface roughness	ξ_{rough}	$2.7336 \cdot 10^6$	0.16 %	$3.9914 \cdot 10^6$	0.11 %	$1.0173 \cdot 10^7$	0.19 %
Power curve	ξ_{power}	$5.6519 \cdot 10^7$	3.29 %	$2.6036 \cdot 10^8$	7.45 %	$2.6928 \cdot 10^8$	5.14 %
Plant performance	$\xi_{\text{performance}}$	$7.3561 \cdot 10^7$	4.28 %	$2.862 \cdot 10^8$	8.19 %	$2.9539 \cdot 10^8$	5.64 %

Table 6.: Results of the variance-based sensitivity analysis of AEP calculation with 10^6 samples using the quasi-Monte Carlo Method.

5.2. *Levelized Costs of Electricity*

In Figure 14 the results regarding the levelized costs of electricity for all nine influencing uncertainty parameters are shown, according to an equal deviation of 5 % (*academic test case*) and according to the deviations given in Table 4 (*realistic test case*).

As before, it can be seen that the uncertainty of wind speed causes the main impact. Another interesting result is that the outliers of the combined and wind speed box plot only spread in the direction of a higher LCOE, which again speaks for the high sensitivity of the wind speed.

Table 7 and Table 8 show the results in terms of the variance-based sensitivity analysis for the academic and realistic test case. Because the LCOE highly depends on the AEP, the uncertainties show a similar behavior as before. In the realistic test case, for all three wind farms the sensitivity is higher than 78 %, while the sensitivities of the power curve and plant performance follow with about 3 to 8 percent. Furthermore, the sensitivities for the capital costs and the annual O& M costs are in-between 1.4 and 7.7 percent. All remaining uncertainties (wake effect, C_t curve, surface roughness, and discount rate) are below 1.2 % and thus have a rather negligible influence on the variance of the model output.

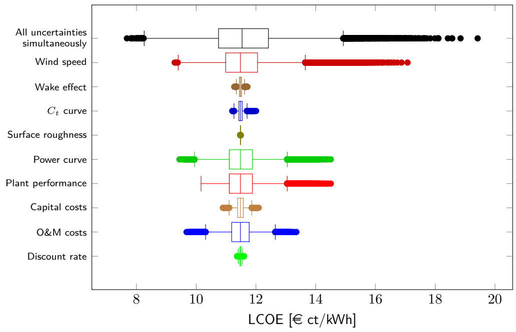

(a) Horns Rev 1 test case with equal deviations of 5 %.

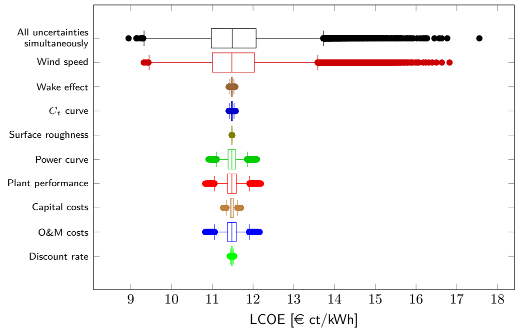

(b) Horns Rev 1 test case with different deviations according to Table 4.

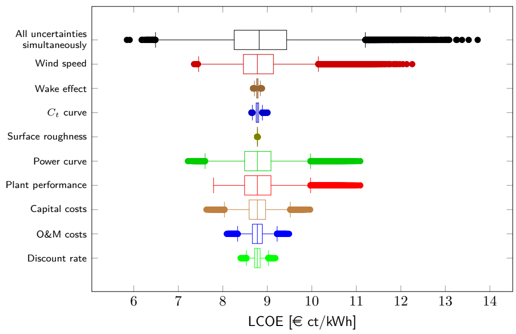

(c) DanTysk test case with equal deviations of 5 %.

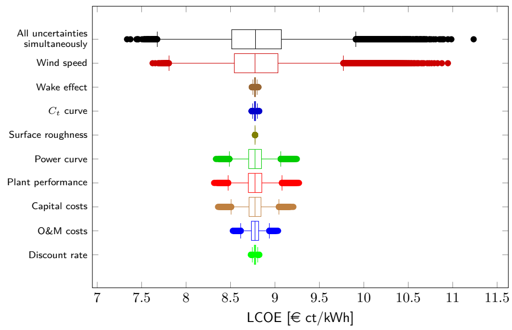

(d) DanTysk test case with different deviations according to Table 4.

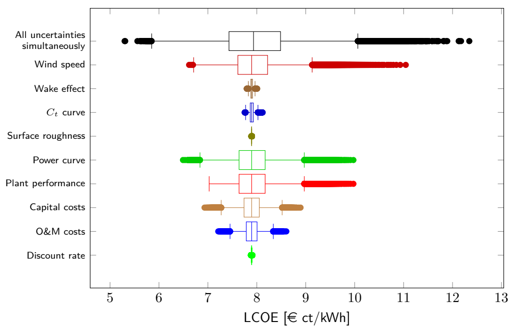

(e) Sandbank test case with equal deviations of 5 %.

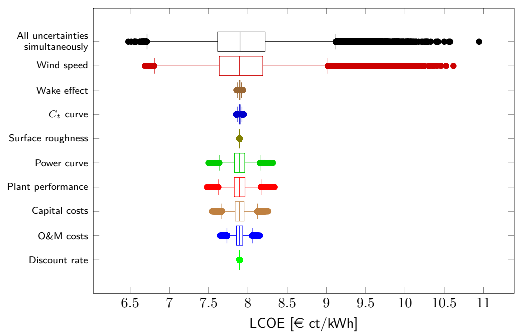

(f) Sandbank test case with different deviations according to Table 4.

Figure 14.: Graphical visualization of the sensitivity analysis with all nine uncertainty parameters wind speed, wake effect, C_t curve, surface roughness, power curve, plant performance, capital costs, O&M costs, and discount rate compared at the same time (simultaneously) to single effects of the uncertainty parameters computed with the quasi-Monte Carlo method with 10^6 samples for the Horns Rev 1, DanTysk, and Sandbank wind farms.

Uncertainty		**Horns Rev 1**		**DanTysk**		**Sandbank**	
		variance	sensitivity	variance	sensitivity	variance	sensitivity
Wind speed	ξ_{wind}	$6.7186 \cdot 10^{-1}$	42.13 %	$2.6737 \cdot 10^{-1}$	33.94 %	$2.1755 \cdot 10^{-1}$	34.53 %
Wake effect	ξ_{wake}	$2.6063 \cdot 10^{-2}$	1.63 %	$1.1135 \cdot 10^{-2}$	1.41 %	$9.4152 \cdot 10^{-3}$	1.49 %
C_t curve	ξ_{ct}	$2.7456 \cdot 10^{-2}$	1.72 %	$1.1165 \cdot 10^{-2}$	1.42 %	$9.6657 \cdot 10^{-3}$	1.53 %
Surface roughness	ξ_{rough}	$2.3825 \cdot 10^{-2}$	1.49 %	$1.0576 \cdot 10^{-2}$	1.34 %	$8.8553 \cdot 10^{-3}$	1.41 %
Power curve	ξ_{power}	$3.4543 \cdot 10^{-1}$	21.66 %	$1.9984 \cdot 10^{-1}$	25.37 %	$1.6189 \cdot 10^{-1}$	25.69 %
Plant performance	$\xi_{\text{performance}}$	$3.433 \cdot 10^{-1}$	21.53 %	$1.9832 \cdot 10^{-1}$	25.18 %	$1.6045 \cdot 10^{-1}$	25.47 %
Capital costs	ξ_{capital}	$4.3827 \cdot 10^{-2}$	2.75 %	$8.5743 \cdot 10^{-2}$	10.88 %	$6.2208 \cdot 10^{-2}$	9.87 %
Annual O&M costs	$\xi_{\text{o\&m}}$	$2.1092 \cdot 10^{-1}$	13.23 %	$3.7667 \cdot 10^{-2}$	4.78 %	$3.5661 \cdot 10^{-2}$	5.66 %
Discount rate	ξ_{rate}	$2.4519 \cdot 10^{-2}$	1.54 %	$1.8883 \cdot 10^{-2}$	2.4 %	$8.8718 \cdot 10^{-3}$	1.41 %

Table 7.: Results of variance-based sensitivity analysis where all uncertainties are fixed to 5 % of LCOE calculation with 10^6 samples using the quasi-Monte Carlo Method.

Uncertainty		**Horns Rev 1**		**DanTysk**		**Sandbank**	
		variance	sensitivity	variance	sensitivity	variance	sensitivity
Wind speed	ξ_{wind}	$6.3759 \cdot 10^{-1}$	90.15 %	$1.3795 \cdot 10^{-1}$	78.52 %	$1.7992 \cdot 10^{-1}$	85.92 %
Wake effect	ξ_{wake}	$8.1103 \cdot 10^{-3}$	1.15 %	$1.0691 \cdot 10^{-3}$	0.61 %	$1.9739 \cdot 10^{-3}$	0.94 %
C_t curve	ξ_{ct}	$8.0655 \cdot 10^{-3}$	1.14 %	$1.0721 \cdot 10^{-3}$	0.61 %	$1.9698 \cdot 10^{-3}$	0.94 %
Surface roughness	ξ_{rough}	$7.8208 \cdot 10^{-3}$	1.11 %	$9.9291 \cdot 10^{-4}$	0.57 %	$1.8982 \cdot 10^{-3}$	0.91 %
Power curve	ξ_{power}	$2.6861 \cdot 10^{-2}$	3.8 %	$1.2308 \cdot 10^{-2}$	7.01 %	$1.0983 \cdot 10^{-2}$	5.24 %
Plant performance	$\xi_{\text{performance}}$	$3.2909 \cdot 10^{-2}$	4.65 %	$1.3451 \cdot 10^{-2}$	7.66 %	$1.19 \cdot 10^{-2}$	5.68 %
Capital costs	ξ_{capital}	$1.0469 \cdot 10^{-2}$	1.48 %	$1.0952 \cdot 10^{-2}$	6.23 %	$8.9661 \cdot 10^{-3}$	4.28 %
Annual O&M costs	$\xi_{\text{o\&m}}$	$3.2609 \cdot 10^{-2}$	4.61 %	$4.5816 \cdot 10^{-3}$	2.61 %	$5.4487 \cdot 10^{-3}$	2.6 %
Discount rate	ξ_{rate}	$7.9749 \cdot 10^{-3}$	1.13 %	$1.1177 \cdot 10^{-3}$	0.64 %	$1.8975 \cdot 10^{-3}$	0.91 %

Table 8.: Results of variance-based sensitivity analysis of LCOE calculation with 10^6 samples using the quasi-Monte Carlo Method.

6. Discussion of the Results

For the three existing wind farms *Horns Rev 1*, *DanTysk*, and *Sandbank* a sensitivity analysis with regard to the two different objective functions AEP and LCOE was performed. For the deviation of the uncertainty-inflicted parameters, we chose two different settings: academic and realistic test cases.

The wind speed has the largest impact with a sensitivity higher than 78 %. This result shows that the assessment of the wind resource is of very high importance. This effect can also be seen in the convergence plot of the UQ methods in Figure 9, as quasi-Monte Carlo and Stochastic Collocation show faster convergence than expected.

The uncertain parameters describing the wake effect, C_t curve, surface roughness, and discount rate have a sensitivity below 1.2 %. In further investigations, these values should not be considered anymore to save computation time. The other four sensitivities for power curve, plant performance, capital costs, and annual O&M costs are in-between 1.4 and 9 % and could therefore be considered in further investigations.

As for UQ methods, quasi-Monte Carlo and Stochastic Collocation show the fastest convergence rates. For ease of implementation and fine-grained error control, we recommend the quasi-Monte Carlo method.

7. Conclusion

Within this work we investigated the sensitivity of certain input parameters for the estimated economics of offshore wind farms. We developed a model describing the wind, wake, and power generation of an offshore wind farm which delivers an output of two economic goal functions, i.e. the AEP and the LCOE. These goal functions are usually used for site evaluation and construction feasibility. We extended the deterministic model by introducing nine uncertain model parameters, e.g. uncertain wind speed and wake effects. Due to the nature of the resulting stochastic model, solution methods from the field of Uncertainty Quantification are needed. Several methods were compared in terms of convergence rate, overhead, and ease of implementation.

As a result of this investigation, the quasi-Monte Carlo was used for the propagation of uncertainties in a wind farm simulation. This is due to the method offering fast convergence rates, low implementation efforts, and good error control.

In a case study we performed a sensitivity analysis on three existing wind farms, i.e. Horns Rev 1, DanTysk, and Sandbank. We investigated the influence of our nine uncertainty-inflicted parameters on two economic quantities.

Our results show that for all wind farms and for all objective functions, wind speed has the largest influence on the variance of the model output. Furthermore, four more parameters could be considered for further sensitivity analyses, while the remaining four parameters are negligible.

Acknowledgements

The authors thank the Federal Ministry for Economic Affairs and Energy BMWi (Bundesministerium für Wirtschaft und Energie) and the Project Executing Organization PTJ (Projektträger Jülich) for making the FINO3 data available. The authors thank Adam Verhoeven-Mrosek from Vattenfall Europe Windkraft GmbH for making offshore wind farm data available.

Disclosure Statement

The author declare that there is no conflict of interest.

References

Ainslie, J. F. (1988). Calculating the flowfield in the wake of wind turbines. *Journal of Wind Engineering and Industrial Aerodynamics*, *27*(1-3), 213–224.

Ashuri, T., Zhang, T., Qian, D., & Rotea, M. (2016). Uncertainty quantification of the levelized cost of energy for a 20 MW research wind turbine model. In *34th wind energy symposium* (p. 1998).

Babuška, I., Nobile, F., & Tempone, R. (2007). A stochastic collocation method for elliptic partial differential equations with random input data. *SIAM Journal on Numerical Analysis*, *45*(3), 1005–1034.

Barthelmie, R., Frandsen, S., Hansen, K., Schepers, J., Rados, K., Schlez, W., . . . Neckelmann, S. (2009). Modelling the impact of wakes on power output at Nysted and Horns Rev. In *European wind energy conference* (pp. 1–10).

Barthelmie, R., Larsen, G., Frandsen, S., Folkerts, L., Rados, K., Pryor, S., . . . Schepers, G. (2006). Comparison of wake model simulations with offshore wind turbine wake profiles measured by sodar. *Journal of atmospheric and oceanic technology*, *23*(7), 888–901.

Bratley, P., & Fox, B. L. (1988). Algorithm 659: Implementing Sobol's quasirandom sequence generator. *ACM Transactions on Mathematical Software (TOMS)*, *14*(1), 88–100.

Brower, M., & Robinson, N. (2012). *The openwind deep-array wake model* (Tech. Rep.). 463 New Karner Road, Albany, NY 12205: AWS Truepower.

Caflisch, R. E. (1998). Monte carlo and quasi-Monte Carlo methods. *Acta numerica*, *7*, 1–49.

Carrillo, C., Cidrás, J., Díaz-Dorado, E., & Obando-Montaño, A. F. (2014). An approach to determine the weibull parameters for wind energy analysis: The case of Galicia (Spain). *Energies*, *7*(4), 2676–2700.

Çakar, R. (2017). *Uncertainty quantification of wind farm models* (Bachelor Thesis). RWTH Aachen University.

de Cursi, E. S., & Sampaio, R. (2015). *Uncertainty quantification and stochastic modeling with Matlab*. Elsevier.

DNV. (2013). *Framework for the categorisation of losses and uncertainty for wind energy assessments* (Tech. Rep.). Høvik, Bærum, Akershus, Norway: KEMA.

Foti, D., Yang, X., & Sotiropoulos, F. (2017). Uncertainty quantification of infinite aligned wind farm performance using non-intrusive polynomial chaos and a distributed roughness model. *Wind Energy*, *20*(6), 945–958.

Gaumond, M., Réthoré, P.-E., Ott, S., Pena, A., Bechmann, A., & Hansen, K. S. (2014). Evaluation of the wind direction uncertainty and its impact on wake modeling at the Horns Rev offshore wind farm. *Wind Energy*, *17*(8), 1169–1178.

Ghanem, R., Higdon, D., & Owhadi, H. (2017). *Handbook of uncertainty quantification*. Springer.

González, J. S., Rodríguez, A. G., Mora, J. C., Santos, J. R., & Payán, M. B. (2009). A new tool for wind farm optimal design. In *Powertech, 2009 ieee bucharest* (pp. 1–7).

Heiming, G. (2015). *Modeling and simulation of offshore wind farms* (Bachelor Thesis). RWTH Aachen University.

Jensen, L., Mørch, C., Sørensen, P., & Svendsen, K. (2004). Wake measurements from the

Horns Rev wind farm. In *European wind energy conference* (pp. 1–9).

Jensen, N. O. (1983). *A note on wind generator interaction* (No. 2411). Risø National Laboratory, Rosklide.

Katic, I., Højstrup, J., & Jensen, N. O. (1986). A simple model for cluster efficiency. In *European wind energy association conference and exhibition* (pp. 407–410).

Lackner, M. A., & Elkinton, C. N. (2007). An analytical framework for offshore wind farm layout optimization. *Wind Engineering*, *31*(1), 17–31.

Lange, B., Larsen, S., Højstrup, J., & Barthelmie, R. (2004). Importance of thermal effects and sea surface roughness for offshore wind resource assessment. *Journal of wind engineering and industrial aerodynamics*, *92*(11), 959–988.

Lange, B., Waldl, H.-P., Guerrero, A. G., Heinemann, D., & Barthelmie, R. J. (2003). Modelling of offshore wind turbine wakes with the wind farm program FLaP. *Wind Energy*, *6*(1), 87–104.

Larsen, G. C., Madsen, H. A., Bingöl, F., Mann, J., Ott, S., Sørensen, J. N., ... others (2007). Dynamic wake meandering modeling. *Risø National Laboratory, Technical University of Denmark, Roskilde, Denmark, Risø*.

Li, S., & Caracoglia, L. (2020). Wind tunnel experimental variability of aerodynamic loads for wind turbine blades. In *Journal of physics: Conference series* (Vol. 1452, p. 012054).

Matsumoto, M., & Nishimura, T. (1998). Mersenne twister: a 623-dimensionally equidistributed uniform pseudo-random number generator. *ACM Transactions on Modeling and Computer Simulation (TOMACS)*, *8*(1), 3–30.

Morokoff, W. J., & Caflisch, R. E. (1995). Quasi-Monte Carlo integration. *Journal of computational physics*, *122*(2), 218–230.

Murcia, J. P., Réthoré, P.-E., Hansen, K. S., Natarajan, A., & Sørensen, J. D. (2015). A new method to estimate the uncertainty of AEP of offshore wind power plants applied to Horns Rev 1. In *Ewea annual conference and exhibition 2015* (pp. 161–165).

Niederreiter, H. (1992). *Random number generation and quasi-Monte Carlo methods.* Siam.

Ott, S. (2009). Fast linearized models for wind turbine wakes. In *Euromech colloquium* (pp. 11–13).

Padrón, A., Stanley, A. P., Thomas, J., Alonso, J., & Ning, A. (2016). Polynomial chaos for the computation of annual energy production in wind farm layout optimization. In *Journal of physics: Conference series* (Vol. 753, p. 032021).

Pillai, A., Chick, J., & Laleu, V. (2014). Modelling wind turbine wakes at middelgrunden wind farm. In *Proceedings of european wind energy conference & exhibition* (pp. 1–10).

Rinker, J. M. (2016). Calculating the sensitivity of wind turbine loads to wind inputs using response surfaces. In *Journal of physics: Conference series* (Vol. 753, p. 032057).

Saltelli, A., Annoni, P., Azzini, I., Campolongo, F., Ratto, M., & Tarantola, S. (2010). Variance based sensitivity analysis of model output. Design and estimator for the total sensitivity index. *Computer Physics Communications*, *181*(2), 259–270.

Schepers, J. (2003). *ENDOW: Validation and improvement of ECN's wake model.* Energy research Centre of the Netherlands ECN.

Smith, R. C. (2013). *Uncertainty quantification: theory, implementation, and applications.* Siam.

Stovall, T., Pawlas, G., & Moriarty, P. (2010). Wind farm wake simulations in OpenFOAM. In *48th aiaa aerospace sciences meeting including the new horizons forum and aerospace exposition* (p. 825).

Sullivan, T. J. (2015). *Introduction to uncertainty quantification.* Springer.

Tuzuner, A., & Yu, Z. (2008). A theoretical analysis on parameter estimation for the weibull wind speed distribution. In *Power and energy society general meeting-conversion and delivery of electrical energy in the 21st century, 2008 ieee* (pp. 1–6).

van Wyk, H.-W., Gunzburger, M. D., & Burkardt, J. (2016). Clenshaw-Curtis type rules for statistical integrals..

Wiernga, J. (1993). Representative roughness parameters for homogeneous terrain. *Boundary-Layer Meteorology*, *63*(4), 323–363.

Wolters, J. (2016). *Uncertainty quantification of wind farm models* (Unpublished master's thesis). RWTH Aachen University.